Low-field galvanomagnetic properties of aluminium-based dilute alloys

1997 J. Phys.: Condens. Matter 9 8997

(http://iopscience.iop.org/0953-8984/9/42/014)

J. Phys.: Condens. Matter **9** (1997) 8997–9006. Printed in the UK PII: S0953-8984(97)82646-X

Low-field galvanomagnetic properties of aluminium-based dilute alloys

Ph Mavropoulos and N Stefanou

Section of Solid State Physics, University of Athens, Panepistimioupolis, GR-157 84 Zografos, Athens, Greece

Received 17 March 1997, in final form 30 July 1997

Abstract. We report a systematic study of low-field galvanomagnetic properties of aluminium-based dilute alloys with 3d and 4sp impurities. The low-field magnetoresistivity tensor is determined by exactly solving the linearized Boltzmann equation for the anisotropic vector mean free path, without using any adjustable parameter. Our method of calculation is based on the on-Fermi-sphere approximation which allows us to combine the full anisotropy of the host Fermi surface, obtained by the four-orthogonal-plane-wave method, with the impurity scattering phase shifts, evaluated by self-consistent local-density-functional impurity-in-jellium calculations. Our results for the Hall coefficient and the magnetoresistance are in good agreement with the experimental data.

1. Introduction

The low-field galvanomagnetic coefficients, like the Hall coefficient and the magnetoresistance, of dilute metallic alloys at low temperatures constitute valuable tools in the investigation of both the topography of the Fermi surface (FS) of the host crystal and the scattering properties of the impurity atoms [1, 2].

In the case of aluminium-based alloys, although the free-electron model predicts a constant Hall coefficient and zero magnetoresistance independent of the nature and strength of the scattering mechanisms, important variations of these quantities with different solute atoms are reported [3–14]. These deviations from the free-electron predictions are mainly due to the scattering of the electronic states of the anisotropic parts of the host FS from the impurity potential and have defied so far a consistent interpretation. Although aluminium is a simple metal with a roughly spherical FS, there are important deviations from the spherical shape with abrupt curvature variations near the Brillouin-zone boundaries. The fact that the detailed structure of these strongly anisotropic regions plays the most decisive role in the determination of the low-field galvanomagnetic coefficients [15] makes the calculation of these quantities cumbersome.

An attempt to calculate low-field galvanomagnetic properties of aluminium-based dilute alloys starting from the self-consistent solution of the linearized Boltzmann equation for an anisotropic transport relaxation time was made by Böning *et al* [13, 14, 16, 17] and by Yonemitsu *et al* [18]. In this approach, the four-orthogonal-plane-wave (4OPW) model was used for the Al host [19], whereas the effective potential of the point defect was described by pseudopotential form factors to first-order Born approximation. However, application of this method was restricted to the case of sp impurities, where the weak-scattering conditions justify the use of the Born approximation.

0953-8984/97/428997+10$19.50

In this article we present a systematic study of low-field galvanomagnetic properties of aluminium containing isolated 3d and 4sp impurities. Our theoretical method relies on the so-called on-Fermi-sphere approximation [20], which allows us to combine the exact topography of the host FS, described by the 4OPW model [19], with the scattering phase shifts, obtained from self-consistent local-density-functional impurity-in-jellium calculations [21]. This method involves an all-electron description of the impurity, which enables us to reliably represent also the case of deep d potentials of the 3d impurity series for which an OPW description is not suitable. Thus, weak sp- as well as strong d-resonance scattering can be treated on the same footing. Within this framework, we calculate the matrix elements of the magnetoresistivity tensor by exactly solving the linearized Boltzmann equation for the anisotropic vector mean free path. For this purpose we use an efficient scheme based on a Jones–Zener-like expansion at low magnetic fields [22], which leads to a hierarchy of integro-differential equations [23], that we solve self-consistently by an iterative procedure. We describe our theoretical method in section 2. Section 3 deals with some technical aspects of the computation and in the last section we present and discuss our results.

2. Theory

We view a sample of the dilute alloy of volume Ω as a single-crystal aluminium matrix with a very small fraction c of its N atomic sites occupied at random by impurity atoms. The magnetoconductivity tensor, $\boldsymbol{\sigma}$, describes the response of this system to a pair of external, homogeneous fields, one electric, $\boldsymbol{\mathcal{E}}$, and one magnetic, $\boldsymbol{B}$. Our approach is based on Boltzmann transport theory. Under the action of the external fields, the system reaches a steady state of dynamical equilibrium through various collision mechanisms. At sufficiently low temperatures, the elastic, incoherent scattering of the FS electrons from isolated impurity atoms is the dominant collision mechanism. The scattering probability rate between two states $|\boldsymbol{k}\rangle$ and $|\boldsymbol{k}'\rangle$ on the FS ($E_{\boldsymbol{k}} = E_{\boldsymbol{k}'} = E_F$) is given by

$$P_{\boldsymbol{k}\boldsymbol{k}'} = \frac{2\pi N c}{\hbar}|T_{\boldsymbol{k}\boldsymbol{k}'}|^2\delta(E_{\boldsymbol{k}} - E_{\boldsymbol{k}'}) \tag{1}$$

where $T_{\boldsymbol{k}\boldsymbol{k}'}$ is the corresponding element of the transition matrix describing the scattering by a single impurity atom.

At not too high electric fields, we can appeal to linear response theory and write the steady state current density, $\boldsymbol{j}$, as

$$\boldsymbol{j} = \boldsymbol{\sigma}(\boldsymbol{B})\boldsymbol{\mathcal{E}}. \tag{2}$$

On the other hand, the current density is determined by the deviation, $g_{\boldsymbol{k}}$, from the Fermi–Dirac distribution function in the absence of external fields, $f^0_{\boldsymbol{k}}$

$$\boldsymbol{j} = \frac{2e}{\Omega}\sum_{\boldsymbol{k}} \boldsymbol{v}_{\boldsymbol{k}} g_{\boldsymbol{k}} \tag{3}$$

where $e = -|e|$ is the electron charge. Comparing (2) with (3) the matrix elements of the magnetoconductivity tensor can be readily deduced. Therefore, the effort should be focused on determining $g_{\boldsymbol{k}}$. To first order in the external electric field, the Boltzmann equation takes the form [24]

$$e(\boldsymbol{v}_{\boldsymbol{k}} \cdot \boldsymbol{\mathcal{E}})\frac{\partial f^0_{\boldsymbol{k}}}{\partial E_{\boldsymbol{k}}} + \frac{e}{\hbar}(\boldsymbol{v}_{\boldsymbol{k}} \times \boldsymbol{B}) \cdot \boldsymbol{\nabla}_{\boldsymbol{k}} g_{\boldsymbol{k}} = \sum_{\boldsymbol{k}'}(g_{\boldsymbol{k}'} - g_{\boldsymbol{k}})P_{\boldsymbol{k}\boldsymbol{k}'} \tag{4}$$

where $\boldsymbol{v}_k = \boldsymbol{\nabla}_k E_k/\hbar$ is the group velocity of Bloch electrons. In the linear-response regime, we seek g_k in the form

$$g_k = -e\frac{\partial f_k^0}{\partial E_k}\boldsymbol{\Lambda}_k(\boldsymbol{B})\cdot\boldsymbol{\mathcal{E}} \tag{5}$$

where $\boldsymbol{\Lambda}_k(\boldsymbol{B})$ represents an anisotropic vector mean free path, which depends on both magnitude and direction of the magnetic field and is, in general, not parallel to the group velocity. Using (1) and (5), (4) is transformed into a inhomogeneous linear, integro-differential equation for $\boldsymbol{\Lambda}_k(\boldsymbol{B})$

$$(c\boldsymbol{\Lambda}_k(\boldsymbol{B})\cdot\boldsymbol{u}_{\mathcal{E}})\frac{\Omega N}{4\pi^2\hbar^2}\int_{FS}\frac{\mathrm{d}S_{k'}}{v_{k'}}|T_{kk'}|^2 = (\boldsymbol{v}_k\cdot\boldsymbol{u}_{\mathcal{E}}) - \frac{e}{\hbar}\left(\boldsymbol{v}_k\times\frac{\boldsymbol{B}}{c}\right)\cdot\boldsymbol{\nabla}_k(c\boldsymbol{\Lambda}_k(\boldsymbol{B})\cdot\boldsymbol{u}_{\mathcal{E}}) + \frac{\Omega N}{4\pi^2\hbar^2}\int_{FS}\frac{\mathrm{d}S_{k'}}{v_{k'}}(c\boldsymbol{\Lambda}_{k'}(\boldsymbol{B})\cdot\boldsymbol{u}_{\mathcal{E}})|T_{kk'}|^2 \tag{6}$$

where $\boldsymbol{u}_{\mathcal{E}}$ is the unit vector along the direction of the electric field. A close inspection of (6) reveals that the quantity $c\boldsymbol{\Lambda}_k(\boldsymbol{B})\cdot\boldsymbol{u}_{\mathcal{E}}$ depends on the magnitude of the magnetic field through the ratio B/c. This form of dependence leads to the so-called Kohler rule [25], which states that the galvanomagnetic coefficients are functions of the effective magnetic field B/c. This scaling law is valid for any crystal symmetry and any magnitude of the magnetic field, as long as quantization of the electron orbits or breakdown phenomena do not occur. In a given dilute alloy, the functional dependence of the galvanomagnetic coefficients on B/c is determined only by the type of defect and by the directions of the external fields, since the defect concentration has been eliminated. Kohler's rule is an exact consequence of the linearized Boltzmann equation and of the assumption for a mechanism of scattering from isolated defects of one specific type.

An efficient method to calculate the low-field magnetoconductivity tensor, avoiding numerical instabilities, is based on the assumption that the quantity $c\boldsymbol{\Lambda}_k(\boldsymbol{B})\cdot\boldsymbol{u}_{\mathcal{E}}$ can be approximated by a power series in the effective magnetic field [22, 23]

$$c\boldsymbol{\Lambda}_k(\boldsymbol{B})\cdot\boldsymbol{u}_{\mathcal{E}} = \varphi_k^{(0)} + (B/c)\varphi_k^{(1)} + (B/c)^2\varphi_k^{(2)} + \cdots. \tag{7}$$

Substituting (7) into (6) and equating terms of the same power of B/c leads to the following hierarchy of equations:

$$\varphi_k^{(0)}\frac{\Omega N}{4\pi^2\hbar^2}\int_{FS}\frac{\mathrm{d}S_{k'}}{v_{k'}}|T_{kk'}|^2 = (\boldsymbol{v}_k\cdot\boldsymbol{u}_{\mathcal{E}}) + \frac{\Omega N}{4\pi^2\hbar^2}\int_{FS}\frac{\mathrm{d}S_{k'}}{v_{k'}}|T_{kk'}|^2\varphi_{k'}^{(0)} \tag{8a}$$

$$\varphi_k^{(1)}\frac{\Omega N}{4\pi^2\hbar^2}\int_{FS}\frac{\mathrm{d}S_{k'}}{v_{k'}}|T_{kk'}|^2 = -\frac{e}{\hbar}(\boldsymbol{v}_k\times\boldsymbol{u}_3)\cdot\boldsymbol{\nabla}_k\varphi_k^{(0)} + \frac{\Omega N}{4\pi^2\hbar^2}\int_{FS}\frac{\mathrm{d}S_{k'}}{v_{k'}}|T_{kk'}|^2\varphi_{k'}^{(1)} \tag{8b}$$

$$\varphi_k^{(2)}\frac{\Omega N}{4\pi^2\hbar^2}\int_{FS}\frac{\mathrm{d}S_{k'}}{v_{k'}}|T_{kk'}|^2 = -\frac{e}{\hbar}(\boldsymbol{v}_k\times\boldsymbol{u}_3)\cdot\boldsymbol{\nabla}_k\varphi_k^{(1)} + \frac{\Omega N}{4\pi^2\hbar^2}\int_{FS}\frac{\mathrm{d}S_{k'}}{v_{k'}}|T_{kk'}|^2\varphi_{k'}^{(2)} \tag{8c}$$

$$\vdots$$

where $\boldsymbol{u}_3$ is the unit vector in the direction of $\boldsymbol{B}$ (x_3 direction). The system of equations (8) can be solved as follows. We first solve (8*a*) by iterations [26] and calculate $\varphi_k^{(0)}$. Using the result for $\varphi_k^{(0)}$, (8*b*) can be solved iteratively to deduce $\varphi_k^{(1)}$, etc. In principle one could continue this procedure to obtain higher-order approximations for the mean free path, but $\varphi_k^{(0)}$, $\varphi_k^{(1)}$ and $\varphi_k^{(2)}$ suffice for the calculation of the low-field magnetoconductivity tensor to leading order in the effective magnetic field. The direction of the electric field obviously influences $\varphi_k^{(0)}$ and then $\varphi_k^{(1)}$ and $\varphi_k^{(2)}$ through the gradient terms, whereas the direction of the magnetic field influences only $\varphi_k^{(1)}$ and $\varphi_k^{(2)}$.

Substituting (7) into (5), and using the resulting expression for $g_{\boldsymbol{k}}$ in (3), we obtain a power-series expansion for the magnetoconductivity tensor

$$\sigma_{ij}(\boldsymbol{B}) = \frac{1}{c}\{\sigma_{ij}^{(0)} + (B/c)\sigma_{ij}^{(1)} + (B/c)^2\sigma_{ij}^{(2)} + \cdots\} \tag{9}$$

with

$$\sigma_{ij}^{(n)} = \frac{2e^2}{(2\pi)^3\hbar}\int_{FS}\frac{\mathrm{d}S_{\boldsymbol{k}}}{v_{\boldsymbol{k}}}(\boldsymbol{v}_{\boldsymbol{k}})_i(\varphi_{\boldsymbol{k}}^{(n)})_j \tag{10}$$

where $(\varphi_{\boldsymbol{k}}^{(n)})_j$ is the appropriate solution of (8) with the electric field oriented in the x_j direction. Having calculated the magnetoconductivity tensor up to order $(B/c)^2$, we can find by matrix inversion the magnetoresistivity tensor $\boldsymbol{\rho}(\boldsymbol{B}) = [\boldsymbol{\sigma}(\boldsymbol{B})]^{-1}$.

A quantity measured directly by experiment is the resistivity component associated with the direction of $\boldsymbol{j}$: $[(\boldsymbol{\rho}(\boldsymbol{B})\boldsymbol{j})\cdot\boldsymbol{j}]/j^2$. Its relative difference with respect to the corresponding value of the resistivity in zero magnetic field defines the magnetoresistance, D. Special arrangements of the magnetic field and the current distinguish between longitudinal magnetoresistance, D_L, and transverse magnetoresistance, D_T. If $\boldsymbol{B}$ and $\boldsymbol{j}$ are parallel we obtain D_L by

$$D_L = \frac{\rho_{33}(\boldsymbol{B}) - \rho_{33}(0)}{\rho_{33}(0)}. \tag{11}$$

If $\boldsymbol{B}$ and $\boldsymbol{j}$ are orthogonal, taking $\boldsymbol{j}$ in the x_1 direction, D_T is obtained from

$$D_T = \frac{\rho_{11}(\boldsymbol{B}) - \rho_{11}(0)}{\rho_{11}(0)}. \tag{12}$$

Furthermore the Hall coefficient, R_H, is given by

$$R_H = \frac{(\boldsymbol{\rho}(\boldsymbol{B})\boldsymbol{j})\cdot(\boldsymbol{B}\times\boldsymbol{j})}{j^2B^2} = \frac{\rho_{21}(\boldsymbol{B})}{B}. \tag{13}$$

In crystals with cubic symmetry we have $\sigma_{ij}^{(0)}/c = \sigma_0\delta_{ij}$. Moreover from Onsager's reciprocity relation $\sigma_{ij}(\boldsymbol{B}) = \sigma_{ji}(-\boldsymbol{B})$ [27] it follows that the diagonal elements of $\sigma_{ij}^{(1)}$ vanish. Taking these two properties into account, we obtain that in the low-field limit R_H tends to a constant, R_H^0, whereas D is proportional to $(B/c)^2$. Since the residual resistivity in zero magnetic field, ρ_0, (isotropic for cubic crystals) is proportional to the defect concentration, one usually uses ρ_0, instead of c, to scale the magnetic field. Thus we write

$$D_L = P_L(B/\rho_0)^2 \tag{14}$$

$$D_T = P_T(B/\rho_0)^2. \tag{15}$$

If the magnetoconductivity tensor is expanded as a power series in the magnetic field, with a view to characterizing the behaviour at low fields, the most general form allowed in a cubic crystal, up to the quadratic terms, can be written [28]

$$\boldsymbol{j} = \sigma_0\boldsymbol{\mathcal{E}} + \sigma_\alpha^{(1)}\boldsymbol{\mathcal{E}}\times\boldsymbol{B} + \sigma_\alpha^{(2)}B^2\boldsymbol{\mathcal{E}} + \sigma_\beta^{(2)}(\boldsymbol{\mathcal{E}}\cdot\boldsymbol{B})\boldsymbol{B} + \sigma_\gamma^{(2)}\mathbf{T}\boldsymbol{\mathcal{E}} \tag{16}$$

where the coefficients $\sigma_\alpha^{(1)}$, $\sigma_\alpha^{(2)}$, $\sigma_\beta^{(2)}$ and $\sigma_\gamma^{(2)}$ are independent of the external fields and $\mathbf{T}$ is a 3×3 matrix, diagonal when referred to the cube axes, with the form $T_{ij} = \delta_{ij}B_iB_j$. The first three terms of (16) describe a conductivity tensor that is isotropic with respect to the orientation of the cube axes relative to the magnetic field, the fourth is relevant to

longitudinal but not to transverse magnetoresistance, while the fifth introduces anisotropic contributions. Inverting (16) we obtain up to second order in the magnetic field

$$\boldsymbol{\mathcal{E}} = \rho_0 \boldsymbol{j} + \rho_\alpha^{(1)} \boldsymbol{j} \times \boldsymbol{B} + \rho_\alpha^{(2)} B^2 \boldsymbol{j} + \rho_\beta^{(2)} (\boldsymbol{j} \cdot \boldsymbol{B}) \boldsymbol{B} + \rho_\gamma^{(2)} \mathbf{T} \boldsymbol{j} \tag{17}$$

where $\rho_\alpha^{(1)} = -\sigma_\alpha^{(1)} \rho_0^2$ is the low-field Hall coefficient, R_H^0, and

$$\begin{aligned} \rho_\alpha^{(2)} &= -(\sigma_\alpha^{(2)} + \rho_0 [\sigma_\alpha^{(1)}]^2) \rho_0^2 \\ \rho_\beta^{(2)} &= -(\sigma_\beta^{(2)} - \rho_0 [\sigma_\alpha^{(1)}]^2) \rho_0^2 \\ \rho_\gamma^{(2)} &= -\sigma_\gamma^{(2)} \rho_0^2. \end{aligned} \tag{18}$$

According to (17), both R_H^0 and ρ_0 are isotropic in cubic metals and can be directly compared with experimental results obtained on polycrystalline samples. This is not however the case for the anisotropic coefficients P_L and P_T.

3. Method of calculation

We construct the FS and Bloch wave-functions of the aluminium host by employing the 4OPW model [19], using the Fermi energy and the pseudopotential matrix elements which were fitted by Cole *et al* [29] to the de Haas–van Alphen experimental data of Coleridge and Holtham [30]. The FS of aluminium can be divided into three parts according to their curvature: (i) a free-electron-like portion in the second zone with a slightly negative curvature, which covers most of the FS; (ii) holelike cylinders also in the second zone, just below the Brillouin-zone boundaries, with a high positive curvature, and (iii) toroid-like portions in the third zone with a high negative curvature. The FS integrations involved in (8) and (10) are performed by generating a system of triangles using, per irreducible part (1/48th) of a Brillouin zone, 1001 points on the second zone and 656 points on the third zone, and then applying a first-order integration rule within each triangle. Special care has been taken in the highly curved regions of the FS, by using a denser mesh. The gradient terms in (8) are calculated as follows. For each point $\boldsymbol{k}$ of the FS mesh, we define two neighbouring points, $\boldsymbol{k} \pm \Delta \boldsymbol{k}$ with $\Delta \boldsymbol{k}$ taken in the direction of $\boldsymbol{v}_{\boldsymbol{k}} \times \boldsymbol{u}_3$, and solve equations (8) also for these neighbouring points. The three points are so close that we can assume that they lie on a straight line, neglecting the curvature of the FS. We then employ locally a second-order interpolation for $\varphi_{\boldsymbol{k}}^{(0)}$ and $\varphi_{\boldsymbol{k}}^{(1)}$ and obtain $(\boldsymbol{v}_{\boldsymbol{k}} \times \boldsymbol{u}_3) \cdot \boldsymbol{\nabla}_{\boldsymbol{k}} \varphi_{\boldsymbol{k}}$ at each of these points, to be used in the subsequent equation. Of course, for $\varphi^{(2)}$ only the gradient of $\varphi^{(1)}$ at points $\boldsymbol{k}$ is needed, whereas the gradient of $\varphi^{(0)}$ is needed at the neighbouring points as well. The accuracy of this procedure was tested by increasing the number of neighbouring points and, accordingly, the order of interpolation, and the results were found to be stable to within about 1%.

In order to calculate the transition matrix $T_{\boldsymbol{k}\boldsymbol{k}'}$ we proceed further by using the on-Fermi-sphere approximation, according to which the crystal lattice pseudopotential is ignored during the scattering of the electrons by the impurity atom [20]. Therefore the problem is reduced to the evaluation of the phase shifts, δ_l, associated with the scattering of a single plane wave from the impurity potential. In this approximation the transition matrix is given by

$$T_{\boldsymbol{k}\boldsymbol{k}'} = -\frac{4\sqrt{2}\pi^2 \hbar^3}{m^{3/2} E_F^{1/2} \Omega} \sum_{lm} \exp\{\mathrm{i}\delta_l(E_F)\} \sin \delta_l(E_F) c_{lm}(\boldsymbol{k}) c_{lm}^*(\boldsymbol{k}') \tag{19}$$

where l and m denote angular momentum quantum numbers and $c_{lm}(\boldsymbol{k})$ are expansion coefficients determined from the 4OPW eigenvectors [26].

We obtain the scattering phase shifts by calculating the electronic structure of an isolated impurity in a jellium having the electron density of Al. Within this model, a substitutional impurity is described by creating a spherical hole with the volume of the aluminium Wigner–Seitz cell ($V = 9\pi^2(\hbar^2/2mE_F)^{3/2}$) in the jellium positive background and inserting the nuclear charge of the impurity in the centre of this vacancy. The electronic structure is calculated self-consistently within the framework of density-functional theory, using a Green function technique [21]. Exchange and correlation effects are included through the local-density approximation with the parametrization of Vosko *et al* [31]. A range of perturbing impurity potential $S = 10$ au and an angular momentum cutoff $l_{max} = 3$ are sufficient to obtain adequate convergence in all cases examined.

4. Results and discussion

We calculated the matrix elements of the low-field magnetoresistivity tensor for aluminium-based dilute alloys with 3d and 4sp impurities, using the method described in the previous sections. We considered the external magnetic field oriented in the [001] and in the [111] directions of a single fcc crystal. The symmetry properties of linear transport coefficients have been discussed by Kleiner [32] in a general way. In a cubic system, if the external magnetic field is parallel to the [001] or the [111] crystallographic direction, the magnetoresistivity tensor in the basis ($\boldsymbol{u}_1$, $\boldsymbol{u}_2$, $\boldsymbol{u}_3$) has the following form:

$$\boldsymbol{\rho} = \begin{pmatrix} \rho_\perp & -\rho_H & 0 \\ \rho_H & \rho_\perp & 0 \\ 0 & 0 & \rho_\parallel \end{pmatrix}. \tag{20}$$

In this case, the transverse magnetoresistance equals $(\rho_\perp(\boldsymbol{B}) - \rho_0)/\rho_0$, independently of the direction of the electric field.

Our results for the low-field Hall coefficient turn out to be independent of the direction of the magnetic field, as expected for cubic crystals. The systematic variation of R_H^0 within the considered series of impurities has been extensively analysed in an earlier work [26]. While for 3d impurities R_H^0 is quite insensitive to the phase shifts and slowly increases with the impurity atomic number, in the case of 4sp impurities it is extremely sensitive to the balance between s and p scattering. Thus any attempt to explain the trends in the numerical results for the 4sp impurities becomes meaningless. In figure 1 we show the calculated low-field Hall coefficient for all the 3d impurities, together with the experimental data [3, 4, 13] and the results of a previous calculation [26]. The only difference between previous and present calculations is that the former explicitly assumes that the vector mean free path is parallel to the group velocity of the corresponding Bloch electron states, whereas the present method is free from this approximation. The present results compared with the previous ones show the same trends, although they are systematically somewhat lower. As can be seen from figure 1, the previous results are in better agreement with experiment for Sc, Ti, V, and Cu, while the present ones agree better for the rest of the series. Therefore, taking also into account the experimental uncertainties [33], it is difficult to conclude whether the present more sophisticated method works better, or not.

Figure 2 shows our results for the low-field transverse-magnetoresistance coefficient, for two different directions of the magnetic field: [001] and [111]. We see that all the considered dilute alloys show systematically a higher magnetoresistance when the magnetic field is in the [111] direction than when it is in the [001] direction. Nevertheless the same qualitative trends of P_T can be observed for both directions of the magnetic field. The low-field transverse-magnetoresistance coefficient versus the impurity atomic number

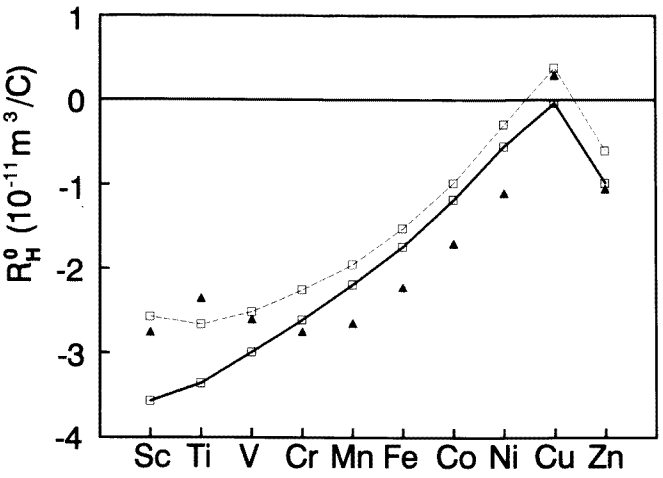

Figure 1. The low-field Hall coefficient of aluminium containing single 3d and 4sp substitutional impurities (solid line). The triangles show the experimental data [3, 4,13]. The broken line shows the results obtained in [26].

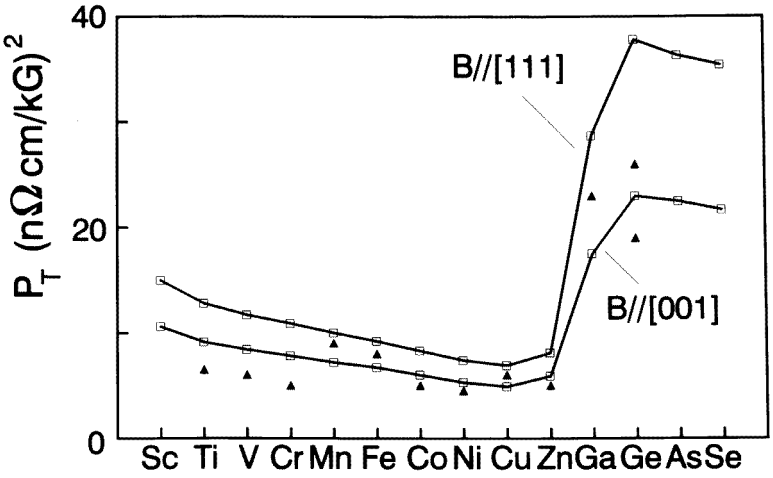

Figure 2. The low-field transverse-magnetoresistance coefficient of aluminium containing single 3d and 4sp substitutional impurities, for two different directions of the magnetic field: [001] and [111] (solid lines). The triangles show the experimental data obtained on polycrystalline samples [4–6, 9, 11].

slowly decreases within the 3d series, then it abruptly increases in the crossover from the 3d to the 4sp series and, finally, it again decreases slowly as we move along the 4sp series.

In the case of 3d impurities, it is reasonable to assume that the impurity is essentially screened by d electrons. Thus, keeping fixed the s and p phase shifts at the Fermi level to their values for Cr impurity and using the actual d phase shifts at E_F, we obtain no appreciable difference in the calculated values of P_T. Therefore we conclude that, in the case of d dominant scattering, small variations of the s and p screening charge do not play an important role.

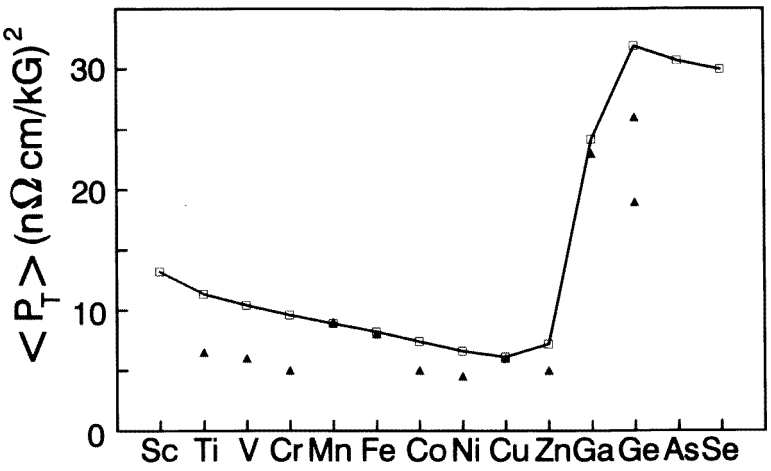

Figure 3. The average low-field transverse-magnetoresistance coefficient of aluminium containing single 3d and 4sp substitutional impurities (solid line). The triangles show the experimental data [4–6, 9, 11].

Setting all the phase shifts at E_F, except one of a given symmetry l_0, equal to zero, the specific form (19) of the transition matrix implies that the quantities $\varphi_{\boldsymbol{k}}^{(n)} \sin^{2n+2} \delta_{l_0}(E_F), n = 0, 1, 2, \ldots$, obtained by solving the hierarchy of equations (8), remain constant, irrespectively of the value of $\delta_{l_0}(E_F)$. Therefore, from (10) it follows that also $\sigma_{ij}^{(n)} \sin^{2n+2} \delta_{l_0}(E_F)$ are constant and, from the definition of the magnetoresistance, it can be shown after some straightforward algebra that a constant P_T is obtained. For the magnetic field in the [001] direction for instance, having only the d phase shift different from zero, we calculate $P_T = 8.4(\text{n}\Omega\ \text{cm kG}^{-1})^2$. This is roughly equal to the low-field transverse-magnetoresistance coefficient in the 3d series of impurities. If only the p phase shift is different from zero we obtain $P_T = 49.7(\text{n}\Omega\ \text{cm kG}^{-1})^2$. This relatively large value of P_T justifies its jump to higher values in the crossover from 3d to 4sp impurities. However, the low-field transverse-magnetoresistance coefficient does not vary in such an abrupt, stepwise manner when we go from d to p dominant scattering. If the contribution of all the scattering channels (s, p, d,...) is taken into account, this transition is smoothed and the results shown in figure 2 are obtained.

In order to compare our results for the low-field magnetoresistance with experimental data obtained on polycrystalline samples, the proper average over all possible orientations of the crystallites with respect to the external fields should be considered. Following Beaulac and Allen [34], such an average is given by [35]

$$\langle P_T \rangle = \rho_0(\rho_\alpha^{(2)} + \tfrac{1}{5}\rho_\gamma^{(2)}) \tag{21a}$$

$$\langle P_L \rangle = \rho_0(\rho_\alpha^{(2)} + \rho_\beta^{(2)} + \tfrac{3}{5}\rho_\gamma^{(2)}) \tag{21b}$$

where $\rho_\alpha^{(2)}$, $\rho_\beta^{(2)}$, and $\rho_\gamma^{(2)}$ are defined through (16), (17) and (18). Using the calculated values of the matrix elements of the magnetoconductivity tensor for the two different directions of the magnetic field that we considered, we can deduce the constant parameters entering in (16) and, consequently, calculate $\langle P_T \rangle$ and $\langle P_L \rangle$ from (21). The results obtained for the average low-field transverse-magnetoresistance coefficient are shown in figure 3. We

can see that $\langle P_T \rangle$ lies between the calculated P_T for $\boldsymbol{B}\|[001]$ and $\boldsymbol{B}\|[111]$, and that the agreement with experiment is good.

As far as the low-field longitudinal magnetoresistance is concerned, there are only limited experimental data available. Yonemitsu *et al* [9] observed that P_L is only just over half of P_T in Al containing Ga, Ge, or Ag impurities. Our calculation confirms qualitatively this observation since we find that, for the impurities that we have considered, the ratio P_T/P_L ranges from 1.5 to 1.7. However, for Ga and Ge we obtain $P_L = 16.6(\text{n}\Omega\ \text{cm kG}^{-1})^2$ and $P_L = 20.6(\text{n}\Omega\ \text{cm kG}^{-1})^2$, respectively, which is somewhat larger than the corresponding measured P_L: $12(\text{n}\Omega\ \text{cm kG}^{-1})^2$ and $14(\text{n}\Omega\ \text{cm kG}^{-1})^2$.

Acknowledgments

The authors would like to thank the General Secretariat for Research and Technology of Greece and the University of Athens for financial support.

References

[1] Hurd C M 1972 *The Hall Effect in Metals and Alloys* (New York: Plenum)
[2] Pippard A B 1989 *Magnetoresistance in Metals* (Cambridge: Cambridge University Press)
[3] Papastaikoudis C and Papadimitropoulos D 1981 *Phys. Rev.* B **24** 3108
[4] Papastaikoudis C, Papadimitropoulos D and Rocofylloy E 1980 *Phys. Rev.* B **22** 2670
[5] Papadimitropoulos D 1983 *PhD Thesis* University of Athens
[6] Papastaikoudis C, Thanou E, Tsamakis D, and Tsefles W 1979 *J. Low Temp. Phys.* **34** 429
[7] Boukos N and Papastaikoudis C 1992 *Phys. Rev.* B **46** 4508
[8] McAlister C P, Hurd C M and Lupton L R 1979 *J. Phys. F: Met. Phys.* **9** 1849
[9] Yonemitsu K, Sato H, Fujita Y and Sakamoto I 1982 *J. Phys. F: Met. Phys.* **12** 2653
[10] Barnard R D and Abdel Rahiem A E E 1981 *Physica* B **107** 505
[11] Rosner P, Sieber G and Böning K unpublished results listed in table 2 of [17]
[12] Kesternich W, Ullmaier H and Schilling W 1976 *J. Phys. F: Met. Phys.* **6** 1867
[13] Böning K, Pfändner K, Rosner P and Schlüter M 1975 *J. Phys. F: Met. Phys.* **5** 1176
[14] Böning K, Pfändner K, Rosner P, Lengeler B and Welter J-M 1979 *Z. Phys.* B **34** 243
[15] Kesternich W 1976 *Phys. Rev.* B **13** 4227
[16] Pfändner K, Böning K and Brenig W 1977 *Solid State Commun.* **23** 31
[17] Pfändner K, Böning K and Brenig W 1979 *Z. Phys.* B **32** 287
[18] Yonemitsu K, Takano K and Matsuda T 1978 *Phys. Status Solidi* B **88** 273
[19] Ashcroft N W 1963 *Phil. Mag.* **8** 2055
Anderson J R and Lane S S 1970 *Phys. Rev.* B **2** 298
[20] Cohen M L and Heine V 1970 *Solid State Physics* vol 24, ed F Seitz, D Turnbull and H Ehrenreich (New York: Academic) pp 37–248
Sorbello R S 1974 *J. Phys. F: Met. Phys.* **4** 1665
[21] Stefanou N and Papanikolaou N 1991 *J. Phys.: Condens. Matter* **3** 3777
[22] Jones H and Zener C 1934 *Proc. R. Soc.* A **145** 268
[23] Taylor P T 1963 *Proc. R. Soc.* A **275** 200
[24] Ziman J M 1972 *Principles of the Theory of Solids* (Cambridge: Cambridge University Press)
[25] Kohler M 1938 *Ann. Phys.* **32** 211
[26] Papanikolaou N, Stefanou N and Papastaikoudis C 1994 *Phys. Rev.* B **49** 16 117
[27] Onsager L 1931 *Phys. Rev.* **37** 405
Onsager L 1931 *Phys. Rev.* **38** 2265
[28] Seitz F 1950 *Phys. Rev.* **79** 372
[29] Cole L, Lawrence W E, Monnier R, Joss W, van der Mark W and Manninen M 1979 *Phys. Rev. Lett.* **42** 1174
[30] Coledidge P T and Holtham P M 1977 *J. Phys. F: Met. Phys.* **7** 1891
[31] Vosko S H, Wilk L and Nusair M 1980 *J. Can. Phys.* **58** 1200
Painter G S 1981 *Phys. Rev.* B **24** 4264
[32] Kleiner W H 1966 *Phys. Rev.* **142** 318

[33] Papastaikoudis C 1996 private communication
[34] Beaulac T P and Allen P B 1983 *Phys. Rev.* B **28** 5439
[35] In the appendix of [34], due to a misprint, $\rho_2^{(2)}$ and $\rho_3^{(2)}$ should be mutually exchanged.